

# Discovery of a Dusty, Chemically Mature Companion to a $z \sim 4$ Starburst Galaxy in JWST ERS Data

BO PENG <sup>1</sup>, AMIT VISHWAS <sup>2</sup>, GORDON STACEY,<sup>1</sup> THOMAS NIKOLA,<sup>2</sup> CODY LAMARCHE <sup>3</sup>, CHRISTOPHER ROONEY <sup>1</sup>,  
CATIE BALL <sup>1</sup>, CARL FERKINHOFF <sup>3</sup>, AND HENRIK SPOON <sup>2</sup>

<sup>1</sup>*Department of Astronomy, Cornell University, Ithaca, NY 14853, USA*

<sup>2</sup>*Cornell Center for Astrophysics and Planetary Science, Cornell University, Ithaca, NY 14853, USA*

<sup>3</sup>*Department of Physics, Winona State University, Winona, MN 55987, USA*

Submitted to ApJ Letter

## ABSTRACT

We report the discovery of two companion sources to a strongly lensed galaxy SPT0418-47 (“ring”) at redshift 4.225, targeted by the JWST Early Release Science program. We confirm that these sources are at a similar redshift as the ring based on  $H\alpha$  detected in the NIRSpec spectrum, and  $[C\ II]\ \lambda 158\ \mu m$  line from ALMA. Using multiple spectral lines detected in JWST/NIRSpec, the rest-frame optical to infrared images from NIRCам and MIRI, and far-infrared (FIR) dust continuum detected by ALMA, we argue that the newly discovered sources are actually lensed images of the same companion galaxy, hereafter referred to as SPT0418-SE (“SE”), located within 5 kpc in the source plane of the ring. The star formation rate derived using  $[C\ II]$  and dust continuum puts a lower limit of  $17\ M_{\odot}/yr$ , while the  $SFR_{H\alpha}$  is estimated to be  $\sim 200$  times lower, thereby confirming that SE is a heavily dust obscured star-forming galaxy. Analysis using optical strong line diagnostics suggests that SE has near solar elemental abundance, while the ring appears to have super-solar metallicity O/H and N/O. We attempt to reconcile the high metallicity in this system by invoking early onset of star formation with continuous high star forming efficiency, or that optical strong line diagnostics need revision at high redshift. We suggest that SPT0418-47 resides in a massive dark matter halo with yet to be discovered neighbors. This work highlights the importance of joint analysis of JWST and ALMA data for a deep and complete picture of the early Universe.

**Keywords:** JWST, High-redshift galaxies, Companion galaxies, Gravitational lensing, Metallicity

## 1. INTRODUCTION

Gravitationally lensed galaxies provide us with unique opportunities to discover and study distant galaxies in detail. Hundreds of ultra luminous infrared galaxies (ULIRGs,  $L_{IR} > 10^{12} L_{\odot}$ ) have been discovered in (sub)millimeter wavelengths (c.f. Ivison et al. 1998; Scott et al. 2008; Weiß et al. 2013; Cañameras et al. 2015). Later studies reveal most of the them as strongly lensed galaxies at high redshift (Spilker et al. 2016; Vieira et al. 2013). These dusty star forming galaxies (DSFG) are characterised by very high star formation rate (SFR) and dust mass, and they are thought to

be the progenitors of massive early type galaxies seen in the local Universe (Casey et al. 2014). The highest SFR systems likely trace the most massive halos in the Universe, and some of these galaxies are later identified as galaxy pairs or proto-clusters (Capak et al. 2011; Aguirre et al. 2013; Marrone et al. 2018; Miller et al. 2018). Studying the stellar population and physical conditions in these galaxies can help us understand how such extremely dusty and massive systems have formed and evolved when the Universe was less than 2 billion years old.

SPT-S J041839-4751.8 (hereafter SPT0418-47) is a DSFG discovered in SPT-SZ survey at redshift 4.2248 (Weiß et al. 2013). Studies using dust continuum and various molecular and fine-structure lines found that SPT0418-47 has very high lensing magnification  $\mu \sim$

32.3 and high intrinsic SFR  $\sim 300 \text{ M}_\odot/\text{yr}$  with a moderate stellar mass  $\sim 1.2 \times 10^{10} \text{ M}_\odot$  (Aravena et al. 2016; Bothwell et al. 2017; De Breuck et al. 2019; Rizzo et al. 2020). It is also included in the JWST Early Release Science program, which for the first time, enables us to study its physical properties in hot ionized gas through optical emission lines, as well as stellar population and distribution. In this paper, we report a serendipitous discovery of a dusty star-forming companion galaxy of SPT0418-47 in JWST/NIRSpec data.

## 2. OBSERVATIONAL DATA

### 2.1. JWST Data

We made use of the JWST dataset targeting SPT0418-47 by the Early Release Science Program TEMPLATES (Targeting Extremely Magnified Panchromatic Lensed Arcs and Their Extended Star formation, ID: 1355, PI: Jane Rigby). We utilized the Stage 3 calibrated data products that were reduced using the JWST pipeline version 1.7.2 and available through the MAST archive.

The dataset consists of a NIRSpec IFU spectral cube, as well as NIRCам and MIRI images. The NIRSpec IFU observation were carried out using the F290LP filter, with wavelength coverage  $2.87\text{--}5.27 \mu\text{m}$ . The target was observed with the NIRCам instrument in six filters (F115W, F150W, F200W, F277W, F356W, F444W) and the MIRI imager in seven filters (F560W, F770W, F1000W, F1280W, F1500W, F1800W, F2100W), providing near continuous photometry from rest-frame  $\lambda_{\text{rest}} = 0.22 \mu\text{m}$  to  $4 \mu\text{m}$ .

For positional alignment, we use the very high S/N dust continuum maps from ALMA with high pointing accuracy. We applied a minor astrometric correction of  $\leq 0''.2$  to the NIRCам images and up to  $0''.5$  in NIRSpec data as well as MIRI images obtained from archive. We also manually flagged bad pixels and resampled the image coordinate grid to facilitate comparison between different bands and instruments.

Extra steps are taken to mitigate the effect of emission from the foreground elliptical galaxy that is lensing the high- $z$  source, outputting lens-subtracted spectral cube and images. The pixels at the centre of the lensing galaxies show calibration artifacts in NIRSpec data, and the core has a bright point source. So, we flagged the pixels within a radius of  $0''.1$  to  $0''.35$  from the center of the lensing galaxy in the first step, depending on the instrument and wavelength. Because the extended emission of the lensing galaxy strongly contaminates the high- $z$  source, we further fit an elliptical Sérsic model for the lensing galaxy and subtracted it from the data. This procedure removes most of the emission of the lens-

ing galaxy, while the compact emission leaves a strong feature resembling the point spread function (PSF) in the lens-subtracted data, especially at short wavelength  $\lambda < 5 \mu\text{m}$ .

### 2.2. ALMA

We use the deep ALMA observations in the data archive (ID:2016.1.01374.S, PI: Hezaveh), which targets SPT0418-47 to study the presence of dark matter substructure through strong lensing measurements. We use the execution block that covers the [C II] fine-structure line ( $^3\text{P}_{3/2} \rightarrow ^3\text{P}_{1/2}$ ,  $\lambda_{\text{rest}} = 157.741 \mu\text{m}$ ,  $\lambda_{\text{obs}} = 824.165 \mu\text{m}$ ).

The source was observed with ALMA on 2016 October 25, using 43 12m antennas with baselines ranging from 18.6m to 1.4km and PWV between 0.65–0.75 mm. Two spectral windows in the upper sideband of the receiver cover the center frequency of the [C II] line ( $\nu_{\text{obs}} = 363.794 \text{ GHz}$ ). The spectral windows in the lower sideband cover a bandwidth of 3.75 GHz around the continuum at rest-frame  $160 \mu\text{m}$ . J0455-4615 and J0439-4522 were observed for amplitude and phase calibration. J0538-4405 was used as the bandpass calibrator and J0519-4546 as the flux calibrator. The integration time for our science target is 32.5 minutes.

The data is retrieved from the ALMA data archive and reduced manually with the Common Astronomy and Software Application (CASA) version 4.7.2 (THE CASA TEAM et al. 2022). We created a continuum map by collapsing the line-free channels covering a bandwidth of 5.47 GHz and using natural weighting. The image is also corrected for the primary beam as the field center specified for the ALMA observations was offset by  $4''.9$  from the location of the target. The resulting image has a beam size of  $0''.18 \times 0''.17$  with a position angle of  $-87.6^\circ$  and achieved a  $1\text{-}\sigma$  sensitivity of  $56 \mu\text{Jy beam}^{-1}$ . We also imaged the line channels separately to create a spectral cube with a  $50 \text{ km s}^{-1}$  resolution, reaching  $1\text{-}\sigma$  noise  $\sim 0.6 \text{ mJy beam}^{-1} \text{ ch}^{-1}$ .

## 3. RESULTS

### 3.1. Discovery

In the pseudo-narrowband image (Fig. 1 left) collapsed over the  $\text{H}\alpha$  line in the original NIRSpec spectral cube, two sources show up in addition to the strongly lensed ring and the lensing elliptical galaxy. The brighter source at the south east corner (“B” in Fig. 1) is referred to as SPT0418-SE-1, and the source between the lensing galaxy and ring (“C”) is denoted SPT0418-SE-2.

The spectra of the newly-discovered sources as well as the strongly-lensed ring (Fig. 1 right) show strong detection of the  $\text{H}\alpha$  line, [N II] $\lambda 6548, 6584$  doublet, [S

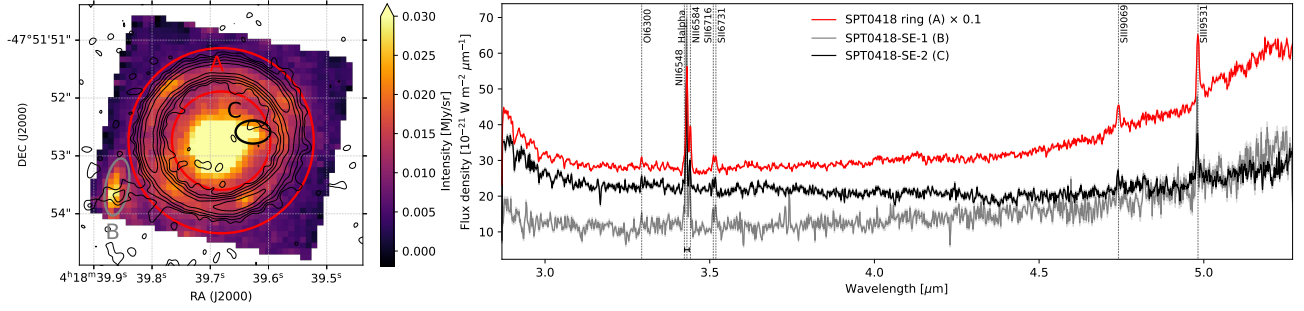


**Figure 1.** Left:  $H\alpha$  pseudo-narrowband image of the SPT0418 system, averaged over the channels including the  $H\alpha$  emission in the original spectral cube. The strongly lensed ring and the two newly discovered sources (SE-1 and SE-2) are highlighted by red annulus, grey and black ellipses, marked as “A”, “B” and “C” respectively. The lensing galaxy is shown as the central bright source. The  $835\ \mu\text{m}$  continuum is plotted as the thin black contour, with the levels  $2, 4, 8, 16, 32 \times \sigma$  where  $\sigma = 56.7\ \mu\text{Jy beam}^{-1}$ . Right: the spectra of the three sources integrated over the regions highlighted in the left panel, using the same colour scheme. The spectrum for the ring is scaled by a factor of 0.1 for clarity. The small black bar below the  $H\alpha$  line marks the wavelength coverage of the pseudo-narrowband image. The potentially detected lines are marked by vertical dotted lines.

$\text{II}]\lambda 6716, 6731$  doublet,  $[\text{S III}]\lambda 9069, 9531$  lines, and a tentative detection of the  $[\text{O I}]\lambda 6300$  line. These strong emission lines enable us to identify the association of the discovered sources in redshift space.

Both SE-1 and SE-2 also appear in NIRCcam and MIRI images at other wavelengths. We also searched in the ALMA data and found that SE-1 appears in the  $835\ \mu\text{m}$  continuum map with a  $\sim 4\sigma$  peak, while SE-2 is associated with a tentative  $2\sigma$  peak (Fig. 1 left contour). Both of them are also detected in the  $[\text{C II}]\lambda 158\ \mu\text{m}$  line.

### 3.2. Observational Properties

We show the moment 0 maps and spectra for the strong lines in Fig. 2. Different from the pseudo-narrowband image, the moment 0 maps are created using the lens-subtracted data, and the continuum is subtracted by a linear fit to the localized spectrum. While the spectra are measured from the lens-subtracted cube with the continuum preserved. The spectra are fitted with Gaussian profile(s) to measure the emission line flux and width. In the fitting procedure, the redshift is fixed relative to that of  $H\alpha$ , and the doublets are fitted as a whole using known emissivity ratio (for  $[\text{N II}]$ ) and the same line width (for the  $[\text{N II}]$  and  $[\text{S II}]$  doublets).

The SE-1 and 2 sources show up strongly in all the moment 0 maps. Remarkably, in the  $H\alpha + [\text{N II}]$  map, SE-1 has an even higher surface brightness than the ring.

In all the spectra, the line peaks of both SE-1 and SE-2 lie consistently at  $-175\ \text{km/s}$  relative to the ring, and the fitted line widths are slightly narrower. But the line center wavelengths and the widths are highly consistent between SE-1 and SE-2 with a line flux ratio about 2:1. One caveat is that the line width of the detections of  $\text{SNR} < 10$  are not well constrained and should not be compared quantitatively. We also caution the absolute

wavelength calibration of NIRSpec data, as the ALMA  $[\text{C II}]$  line is at lower redshift for both the ring and the newly-discovered sources (see table 1).

The 1 to  $10\ \mu\text{m}$  lens-subtracted images are shown in Fig. 3. We note that at short wavelength  $\lambda < 2\ \mu\text{m}$ , SE-1 appears to have a bright nucleus accompanied by two faint patches on both north and south sides. At 2.8 and  $3.6\ \mu\text{m}$  which are strongly affected by the  $[\text{O III}]\lambda 5007$  and  $H\alpha$  emission lines respectively, SE-1 appear more extended, and the surface brightness contrast to the ring are higher compared to other wavelengths. The primary lensed galaxy (ring) also shows extended morphology that agrees with the line maps in Fig. 2. Only the images up to  $10\ \mu\text{m}$  are plotted as the companion sources are barely detectable at longer wavelengths.

The dark hexagon shape present at the center of the short wavelength images is the result of the compact continuum emission from the lensing galaxy (Sec. 2.1). This PSF residual makes the identification and photometry challenging for SE-2. Proper subtraction of the lensing galaxy would require a core model convolved with JWST PSF, which is beyond the scope of this paper.

The basic properties, line fluxes and widths, and photometries of NIRCcam and MIRI images are summarized in Table 1. Line fluxes and full width half maximum (FWHM) are derived from Gaussian fittings.

## 4. DISCUSSION

### 4.1. Nature and Morphology

Based on the redshift, line profile, and spatial separation between the newly identified source and the ring, it is evident that both SE-1 and SE-2 are physically different sources than the primary galaxy of the Einstein ring. However, we further argue that SE-1 and SE-2 are actually two lensed images of the same galaxy: both

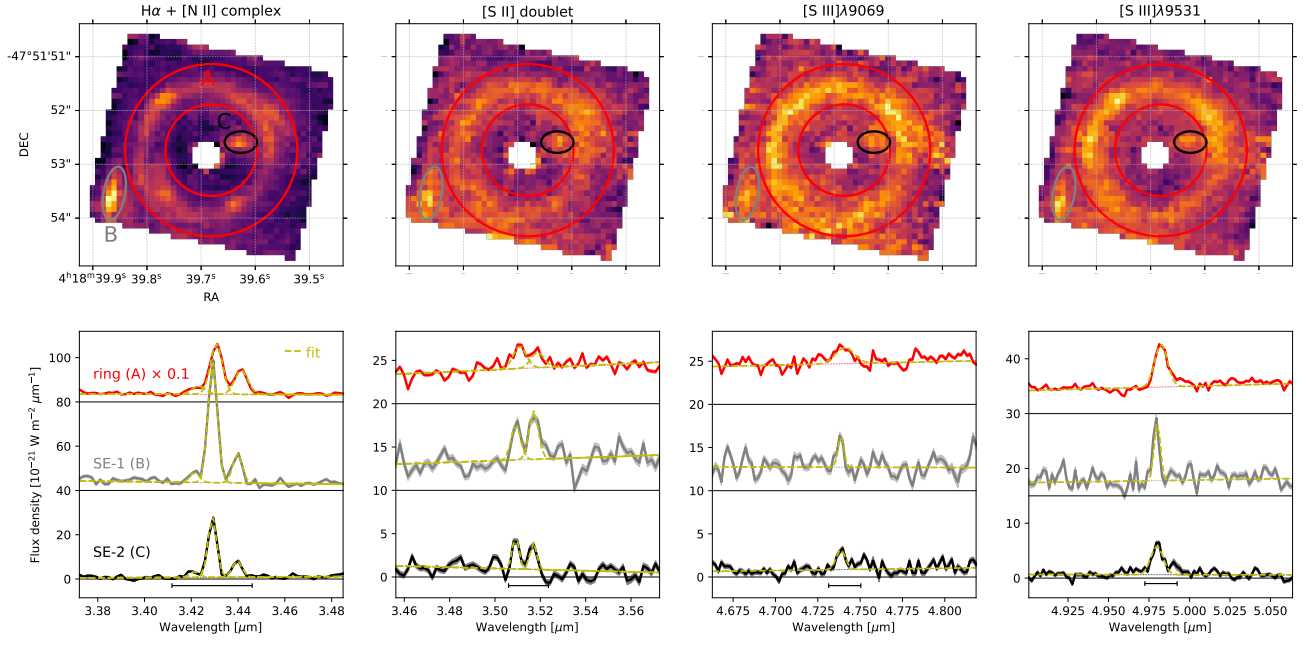


**Figure 2.** The moment 0 map and spectrum snippets of the strong emission lines. For each strong line(s), the lens-subtracted continuum subtracted moment 0 map is displayed in the first row, with the same marked regions as in Fig. 1. The spectrum snippets are shown in the second row, integrated over the three regions. The spectra are offset vertically to aid the vision, with the zero baseline indicated by a thin black line. The yellow dashed line indicates the Gaussian fit to the line or line associations plus the linear fit to the local continuum. The plotting style and colour of the spectrum are the same as Fig. 1.

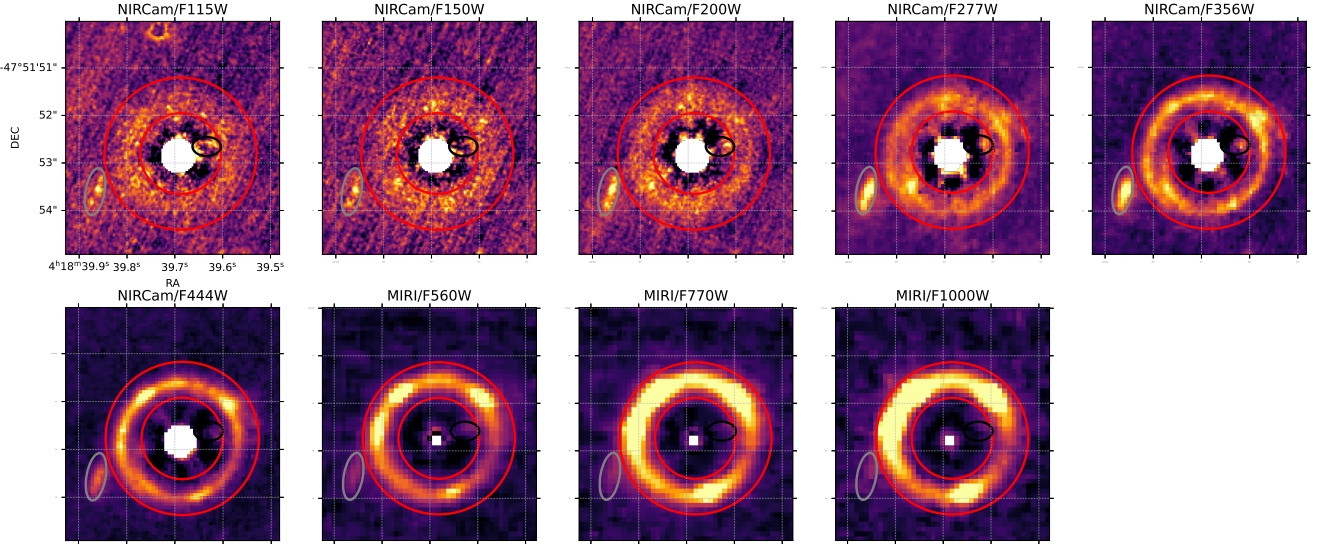


**Figure 3.** Atlas of lens-subtracted NIRCам and MIRI images in the wavelength range  $\lambda_{\text{obs}} = 1.15 - 10 \mu\text{m}$ , corresponding to  $\lambda_{\text{rest}} = 0.22 - 1.9 \mu\text{m}$ . The filter is shown as the title of each stamp. The images are oriented and cropped to fit the image stamps in the previous images, so are the highlighted regions and colour scheme. The colour map is adjusted manually to increase the contrasts of the weak sources.

**Table 1.** Properties of the newly discovered source. The “SE” column is the combined properties of both SE-1 and SE-2, as we speculate that they are the primary and counter lensed image of the same galaxy. For non-detection in SE-2 we report the  $3\sigma$  upper limit, and scale the SE-1 value up by a factor of 1.5 to estimate the value for SE.

	SPT0418-SE-1	SPT0418-SE-2	SPT0418-SE		
R.A. (J2000)	04:18:39.86(1)	04:18:39.63(1)			
Decl. (2000)	-47:51:53.54(5)	-47:51:52.59(5)			
$z_{\text{H}\alpha}$	4.2251	4.2250	4.2251		
$z_{[\text{C II}]}$	4.223	4.223	4.223		
Spectroscopic properties					
line	Flux $10^{-23} \text{ W m}^{-2}$	FWHM $\text{km s}^{-1}$	Flux $10^{-23} \text{ W m}^{-2}$	FWHM $\text{km s}^{-1}$	Flux $10^{-23} \text{ W m}^{-2}$
H $\alpha$	$27.1 \pm 0.50$	409	$12.6 \pm 0.29$	379	$39.7 \pm 0.58$
[N II] $\lambda$ 6548	$2.26 \pm 0.5$	406	$1.26 \pm 0.29$	409	$3.52 \pm 0.58$
[N II] $\lambda$ 6584	$6.72 \pm 0.54$	406	$3.74 \pm 0.30$	409	$10.46 \pm 0.62$
[S II] $\lambda$ 6716	$2.11 \pm 0.47$	404	$1.36 \pm 0.27$	291	$3.47 \pm 0.54$
[S II] $\lambda$ 6731	$2.81 \pm 0.47$	404	$1.14 \pm 0.27$	291	$3.95 \pm 0.54$
[S III] $\lambda$ 9069	$1.57 \pm 0.40$	245	$1.55 \pm 0.30$	404	$3.12 \pm 0.50$
[S III] $\lambda$ 9531	$5.07 \pm 0.56$	269	$4.92 \pm 0.36$	538	$9.99 \pm 0.66$
[C II] $158\mu\text{m}$	$5590 \pm 850$	200	$1770 \pm 360$	200	$7360 \pm 920$
	$(4.6 \pm 0.7 \text{ Jy km/s})$		$(1.46 \pm 0.30 \text{ Jy km/s})$		$(6.06 \pm 0.76 \text{ Jy km/s})$
Photometric properties					
filter	$S_\nu$ $\mu\text{Jy}$	$S_\nu$ $\mu\text{Jy}$	$S_\nu$ $\mu\text{Jy}$	$S_\nu$ $\mu\text{Jy}$	$S_\nu$ $\mu\text{Jy}$
NIRCam/F115w	$0.338 \pm 0.017$		$0.221 \pm 0.045$		$0.559 \pm 0.048$
NIRCam/F150w	$0.490 \pm 0.022$		$0.145 \pm 0.066$		$0.635 \pm 0.070$
NIRCam/F200w	$0.671 \pm 0.020$		$0.129 \pm 0.132$		$0.800 \pm 0.134$
NIRCam/F277w	$0.606 \pm 0.023$		$<0.554$		$0.909 \pm 0.186$
NIRCam/F356w	$0.803 \pm 0.021$		$<0.734$		$1.20 \pm 0.246$
NIRCam/F444w	$0.708 \pm 0.020$		$<0.871$		$1.06 \pm 0.29$
MIRI/F560w	$1.18 \pm 0.081$		$0.435 \pm 0.171$		$1.62 \pm 0.19$
MIRI/F770w	$1.42 \pm 0.127$		$0.319 \pm 0.319$		$1.74 \pm 0.34$
MIRI/F1000w	$1.78 \pm 0.224$		$0.145 \pm 0.491$		$1.92 \pm 0.54$
MIRI/F1280w	$1.21 \pm 0.286$		$<1.28$		$1.82 \pm 0.51$
MIRI/F1500w	$1.07 \pm 0.319$		$<0.987$		$1.60 \pm 0.46$
MIRI/F1800w	$0.874 \pm 0.358$		$<1.19$		$1.31 \pm 0.53$
MIRI/F2100w	$0.788 \pm 0.288$		$<1.02$		$1.18 \pm 0.44$
ALMA/835 $\mu\text{m}$	$733 \pm 227$		$235 \pm 150$		$968 \pm 272$
Derived properties					
$\mu\text{L}_{\text{H}\alpha} [10^8 \text{ L}_\odot]$	$0.129 \pm 0.002$		$0.0598 \pm 0.0014$		$0.189 \pm 0.002$
$\mu\text{L}_{[\text{C II}]} [10^8 \text{ L}_\odot]$	$26 \pm 4.0$		$8.41 \pm 1.72$		$34.4 \pm 4.4$
$\mu\text{L}_{\text{FIR}} [10^{11} \text{ L}_\odot]$	$9.1^{+6.7}_{-3.6}$		$2.9^{+2.7}_{-2.0}$		$12.0^{+8.7}_{-4.5}$
$\mu\text{SFR}_{\text{H}\alpha} [\text{M}_\odot/\text{yr}]$	$0.26 \pm 0.004$		$0.12 \pm 0.003$		$0.38 \pm 0.004$
$\mu\text{SFR}_{[\text{C II}]} [\text{M}_\odot/\text{yr}]$	$65 \pm 10$		$20 \pm 4.2$		$87 \pm 11$
$\mu\text{SFR}_{\text{FIR}} [\text{M}_\odot/\text{yr}]$	$118^{+87}_{-47}$		$38^{+35}_{-26}$		$156^{+113}_{-58}$
$\log(\text{O}/\text{H})_{N2}$	$-3.47 \pm 0.09$		$-3.40 \pm 0.09$		$-3.44 \pm 0.07$
$\log(\text{O}/\text{H})_{S23}$	$-3.60 \pm 0.26$		$-3.26 \pm 0.25$		$-3.47 \pm 0.18$
$\log(\text{N}/\text{O})_{N2S2}$	$-0.69 \pm 0.16$		$-0.64 \pm 0.17$		$-0.67 \pm 0.12$



sources have the same redshift and line width in all the strong lines within the allowance of measurement error; the SE-1 to SE-2 line flux density ratios for all the spectral lines and continuum are roughly 2:1; and both sources are separated from the ring by about  $0''.7$ , in the south east direction.

Therefore, we posit that SE-1 and SE-2 are the primary and counter images of a lensed companion galaxy (hereafter referred to as companion or SE) lensed by the same foreground galaxy as the ring (hereafter as the host galaxy). Based on the separation in the image plane, We can estimate the companion is also within a projected distance of 5 kpc from the host in the source plane. Based on the linear scale of the elongated shape, we estimated that the magnification of SE-1 is at least 8 times smaller than the ring, and at least 16 times smaller than for SE-2. Therefore, using  $\mu \sim 32$  for the ring (Spilker et al. 2016; Rizzo et al. 2020), the upper limit for the total magnification of SE is  $\mu < 6$ .

In addition to the newly discovered companion, there are even more arc-like weak features in NIRCam images beyond the NIRSpc field of view. Future deeper and wider spectroscopic observations may decipher this seemingly crowded field.

The morphology of the companion is intriguing. At short wavelengths, the galaxy displays a nuclear feature, which we will argue in Sec. 4.3 to be a starburst nucleus. The morphology of gas and the old stellar population by  $\lambda_{rest} = 0.8 - 2 \mu\text{m}$  images, are more extended than the dust traced by ALMA continuum and young stellar population by  $\lambda_{rest} \leq 0.4 \mu\text{m}$  images. This dichotomy appears in both the SE-1&2 and the ring, and is consistent with the recent findings that [C II] is often more extended than both UV and dust continuum (Carniani et al. 2018; Fujimoto et al. 2019; Ginolfi et al. 2020; Fudamoto et al. 2022). In addition, there is a dust lane-like gap at the southeast and northwest of the ring in the H $\alpha$  map, 2.8 and 3.6  $\mu\text{m}$  images, suggesting its association with gas emission. We suspect the gaps are regions of very high dust extinction or the line emission is suppressed.

#### 4.2. Dust Obscured Star Formation Rate

We estimated the star formation rate of the companion galaxy in three ways:  $\text{SFR}_{\text{H}\alpha}$  using the formula in Murphy et al. (2011),  $\text{SFR}_{[\text{C II}]}$  using [C II]-SFR relation in Herrera-Camus et al. (2015),  $\text{SFR}_{\text{FIR}}$  using the scaling relation given by Kennicutt (1998). As we have a single point of the dust SED, we estimated the FIR luminosity assuming a  $\beta = 1.8$  and the commonly used 850  $\mu\text{m}$  relation (Genzel et al. 2010; Carilli & Walter 2013). The estimates of SFR are not corrected for lensing and

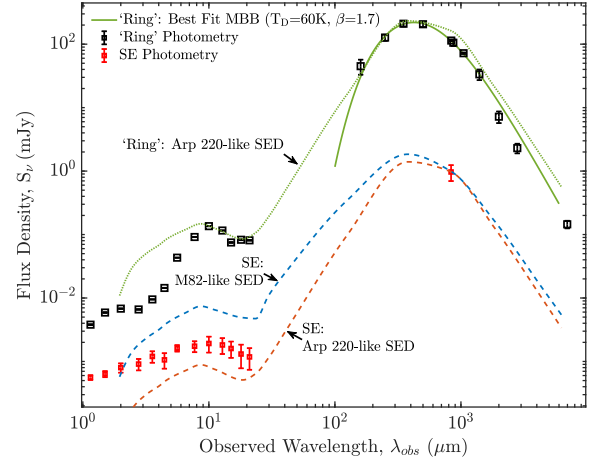


**Figure 4.** SED of SPT0418-47 system (black square) and the companion SE (red square), along with the Arp-220 (red dashed) and M82 (blue dashed) SED templates (Polletta et al. 2008) normalized by the dust continuum, and the best fit modified blackbody (MBB) model for SPT0418-47. The figure is adapted from (Vishwas 2019).

are thus labelled as  $\mu\text{SFR}$ . The results are summarized in Table 1.

We found that while the  $\text{SFR}_{[\text{C II}]}$  agrees with  $\text{SFR}_{\text{FIR}}$  within errors due to the limited fidelity afforded by using a single photometric point, it is a factor of  $\sim 200$  higher than  $\text{SFR}_{\text{H}\alpha}$ . By attributing all the difference between  $\text{SFR}_{[\text{C II}]}$  and  $\text{SFR}_{\text{H}\alpha}$  to dust extinction, we can obtain an obscuration fraction of star formation  $\sim 99.5\%$  for SE. This high obscuration fraction suggests that the companion galaxy is also extremely dusty in nature. Although these instruments are still being calibrated and the absolute flux calibration may be revised in the future, the calibration uncertainty itself is unlikely to resolve the two orders of magnitude difference in SFR.

Using the upper limit of the magnification for the companion galaxy SE, and a reconciled  $\mu\text{SFR} = 100 \text{ M}_{\odot}/\text{yr}$ , we can obtain a lower limit of the intrinsic SFR of  $17 \text{ M}_{\odot}/\text{yr}$ . This intrinsic SFR is about 20 times less than the host galaxy (De Breuck et al. 2019). This securely places SE in the range of typical star-forming galaxies at redshift 4-5 Le Fèvre et al. (2020).

The extreme dust obscuration is also apparent in the spectral energy distribution (SED) in Fig. 4. A large infrared-to-optical excess (IRX) is present at a level comparable to the local ULIRG Arp-220, with  $\text{IRX}=3.4$  (Howell et al. 2010). SE has slightly less obscuration than the host, indicating lower dust mass fraction. This difference in obscuration might be responsible for the higher H $\alpha$  surface brightness in SE-1 than the ring.

Most (U)LIRGs in the local Universe are in the process of merging, which likely triggers the starburst activity in these systems (Sanders & Mirabel 1996; Armus et al. 2009). It is thus natural to speculate SPT0418-47 as an analog of merging (U)LIRGs at high- $z$ . However, due to the small size of the companion and the distortion by gravitational lensing, it requires lens modelling to study the relation between the companion and the host galaxies in 3D. The merger scenario also questions the stability of the dynamically cold disk found by Rizzo et al. (2020), which will be disrupted by the tidal interactions that are commonly seen in the local (U)LIRGs.

#### 4.3. Radiation field

We characterised the radiation field using the Nitrogen and Sulfur lines detected in the NIRSpc spectrum. The  $[\text{N II}]\lambda 6584/\text{H}\alpha$  ratio  $\sim 0.25$  places SE in the star forming locus in BPT diagram with relatively soft radiation (Baldwin et al. 1981; Kewley et al. 2019). This leads to the argument that the compact nuclear feature present in the  $\lambda_{\text{rest}} \leq 5000 \text{ \AA}$  images is more likely a starburst nucleus instead of an AGN. While we can not rule out a low-luminosity AGN being present, the star-formation scenario is further supported by the lack of strong rest-frame UV radiation, dimming in mid-infrared bands, and the high SFR inferred in this galaxy.

The  $S32$  index of  $\log [\text{S III}]/[\text{S II}]$  is primarily a measure of the ionization parameter  $U$ . The shorter wavelength  $[\text{S II}]$  line is more extinguished, so we can only put an upper limit on  $S32$  ratio to be  $\lesssim 0.25$ . We then estimated an upper limit of  $\log U \lesssim -3$  using the diagnostics given in Kewley et al. (2019). This is within the range measured in the local Universe, suggesting similar conditions in the ionized gas of the star forming region (Sanders et al. 2020). The small value of  $U$  also predicts relatively weak  $[\text{O III}]\lambda 4959, 5007$  lines (Strom et al. 2018), as is also suggest by its allowed position on BPT diagram.

#### 4.4. Metallicity

We estimated the chemical abundance in SE using three methods. The absolute abundance  $\text{O}/\text{H}$  is calculated using two strong line methods: the  $N2$  index with the third-order polynomial fit in PP04; and the  $S23$  index in Díaz & Pérez-Montero (2000). We also used the  $N2S2$  index (Viironen et al. 2007; Pérez-Montero & Contini 2009) to measure the Nitrogen-to-Oxygen abundance ratio  $\text{N}/\text{O}$ . The results are recorded in Table 1.

We found SE to be chemically mature with  $\text{O}/\text{H} \sim 0.6$  times the solar abundance and  $\text{N}/\text{O} \sim 1.2$  times solar, which are surprisingly high for a galaxy only 1.46 billion years after the Big Bang. These estimates are robust

because (1) only line ratios are used and they are not affected by the uncertainties in the absolute calibration of JWST; (2) the emission lines are close in wavelength, so the line ratio is not subject to differential extinction, with the only exception being the  $[\text{S III}]$  lines; (3) the three methods use a suite of lines and all reach a consistent result of near-solar metallicity; it would require at least two of the line-flux values to change in order to attain some other consistent results. Systematic uncertainty in these empirical optical diagnostics are typically 0.3 dex (Pérez-Montero & Contini 2009), but it is not included in the error values reported in Table 1 for clarity. However, the systematic error is reduced when combining and comparing different methods.

The near-solar abundance and the elevated  $\text{N}/\text{O}$  ratio, suggests this galaxy hosts highly enriched interstellar medium. It is consistent with the large dust content and relatively soft radiation field in this galaxy. But drawing a comparison with the metallicity of star-forming galaxies at redshift 1 to 3 from ground based observations (c.f. Steidel et al. 2014; Kashino et al. 2017; Strom et al. 2022), both  $\text{O}/\text{H}$  and  $\text{N}/\text{O}$  of SE are at the very high end of the distribution, yet they are at a much earlier epoch in the Universe. This suggests a rare and unusual chemical evolution history for SE.

It is even more striking that an identical analysis on the host galaxy found the metallicity  $Z \sim 1.6 Z_{\odot}$ , and  $(\text{N}/\text{O}) \sim 3 \times (\text{N}/\text{O})_{\odot}$ . This metallicity is even higher than  $Z \sim Z_{\odot}$  derived in De Breuck et al. (2019). Because the gas phase elemental abundance builds up through nuclear synthesis and stellar feedback, and the growth of  $\text{N}/\text{O}$  is slower through the prolonged secondary production of Nitrogen,  $\text{O}/\text{H}$  and  $\text{N}/\text{O}$  abundances strongly constrains the age and star forming efficiency (SFE) of a galaxy. Comparing with the chemical evolution model in Fig. 5 of Vincenzo et al. (2016), SE is inferred to have an age of at least 800 Myr with a preferentially short depletion time scale  $\tau \leq 0.67 \text{ Gyr}$ , while the super-solar metallicity of the host, especially the high  $\text{N}/\text{O}$ , requires the galaxy formation to start shortly after the Big Bang, sustaining a high SFE with  $\tau \leq 0.3 \text{ Gyr}$ .

The high SFE inferred from the metallicity supports a decreasing depletion time towards higher redshift found by other studies (Saintonge et al. 2013; Tacconi et al. 2020). The younger age of the companion suggested by the lower metallicity is also consistent with the lack of  $\lambda_{\text{rest}} \sim 2 \mu\text{m}$  peak in the SED corresponding to the old stellar population, which shows up strongly for the more evolved host galaxy. On the other hand, the inferred early onset of galaxy formation, clustering of galaxies, and the potential crowded field indicates the system

might trace a massive dark matter halo that enables structure formation in a very early time.

Although most of the FIR fine-structure line observations are not resolved for SE, we can still compare the FIR diagnostic of the whole system. In addition to [C II], the system is also detected in [O III] 88  $\mu\text{m}$  and [N II] 122  $\mu\text{m}$  lines (De Breuck et al. 2019). The [N II]122/[O III]88 flux ratio, which can be a rough proxy for N/O, is only 0.05. In the local universe, such a small line ratio is more commonly seen in dwarf galaxies in consequence of both hard stellar radiation fields and low N/O (Cormier et al. 2015), rather than (U)LIRGs (Díaz-Santos et al. 2017) that the dusty and metal rich SPT0418-47 system resembles. The weak [N II] 122 and 205  $\mu\text{m}$  lines are also in contrast to the relatively bright [N II] $\lambda$ 6584 line.

One possible solution is the applicability of the optical strong line diagnostics in the early Universe. Strom et al. (2018) found a slightly modified relation for estimating the elemental abundances using optical spectral lines at redshift 2~3 compared to those from local galaxies. Using the revised  $N2$  and  $N2S2$  calibration in Strom et al. (2018), the N/O of both the host and the companion decrease by about 0.25 dex, corresponding to 1.6 and 1 times the solar abundance respectively. However, we do not find a significant change in the estimate for O/H. Though still high, the new values of N/O need a much less evolved stellar population, and they are closer to the  $\log(\text{N/O}) \sim -1.1$  estimated from the empirical [O III]88/[N II]122-to-N/O relation in the local Universe. We leave more detailed analysis on chemical abundance of the ring to future publications.

## 5. SUMMARY AND FUTURE WORK

In this study, we report the discovery of a dusty star-forming companion galaxy SPT0418-47-SE in the SPT0418-47 system. The companion galaxy is also gravitationally lensed, which results into the two images SE-1 and SE-2. By combining JWST and ALMA observations, we find a high SFR of the companion galaxy with near unity dust obscuration fraction. Using strong line indices we find near-solar and super-solar metallicity for the companion and the host galaxy.

This work highlights the capability of JWST for discovering fainter and lower SFR galaxies in the early Universe. It also shows the value of joint study of both optical and submillimeter observations, as 99.5% SFR of the companion galaxy is obscured by dust. JWST for the first time enables us to study the physical conditions of the hot gas through strong optical lines at  $z > 4$ . This

work illustrates some exciting discoveries and results that are attained with these lines. This spectroscopic study of a  $z > 4$  galaxy opens up many questions including: the spatial arrangement and stellar/gas/metallicity distribution of the companion; the merging hypothesis of SPT0418-47; the dark matter halo of the system; the over-density of this potentially crowded field; reconciling the relatively high chemical abundances with the short formation time and the moderate stellar mass for the whole system; and interpreting the small [N II] 122 and 205  $\mu\text{m}$  luminosities in the context of either a soft radiation field and/or a high N/O.

With solar-like metallicity and clustering signature at a cosmic age of 1.4 Gyr, our work suggests SPT0418-47 is a good example of the very early mass buildup and structure formation. The high lensing factor, rich observational data and the many intriguing questions on its formation history makes it an ideal target for future observations and in-depth study. We therefore call for NIR-Spec observations covering the [O III] $\lambda$ 4959,5007 doublets and [O II] $\lambda$ 3727 lines, an H $\alpha$  narrowband search in the SPT0418-47 field, as well as deep resolved ALMA [N II] and [O III] observations.

This work was supported by the National Science Foundation through the following grants: NRAO SOS 1519126, AST-1716229, CAREER-1847892 and AST-2009767, and NASA/USRA SOFIA grant 09-0185. This work is based on observations made with the NASA/ESA/CSA James Webb Space Telescope. The data were obtained from the Mikulski Archive for Space Telescopes at the Space Telescope Science Institute, which is operated by the Association of Universities for Research in Astronomy, Inc., under NASA contract NAS 5-03127 for JWST. These observations are associated with program 1355. The authors acknowledge the TEMPLATES team led by Jane Rigby for developing their observing program with a zero-exclusive-access period. This paper makes use of the following ALMA data: ADS/JAO.ALMA#2016.1.01374.S ALMA is a partnership of ESO (representing its member states), NSF (USA) and NINS (Japan), together with NRC (Canada), MOST and ASIAA (Taiwan), and KASI (Republic of Korea), in cooperation with the Republic of Chile. The Joint ALMA Observatory is operated by ESO, AUI/NRAO and NAOJ. The National Radio Astronomy Observatory is a facility of the National Science Foundation operated under cooperative agreement by Associated Universities, Inc.

## REFERENCES



- Aguirre, P., Baker, A. J., Menanteau, F., Lutz, D., & Tacconi, L. J. 2013, *ApJ*, 768, 164, doi: [10.1088/0004-637X/768/2/164](https://doi.org/10.1088/0004-637X/768/2/164)
- Aravena, M., Spilker, J. S., Bethérmin, M., et al. 2016, *MNRAS*, 457, 4406, doi: [10.1093/mnras/stw275](https://doi.org/10.1093/mnras/stw275)
- Armus, L., Mazzarella, J. M., Evans, A. S., et al. 2009, *PASP*, 121, 559, doi: [10.1086/600092](https://doi.org/10.1086/600092)
- Baldwin, J. A., Phillips, M. M., & Terlevich, R. 1981, *PASP*, 93, 5, doi: [10.1086/130766](https://doi.org/10.1086/130766)
- Bothwell, M. S., Aguirre, J. E., Aravena, M., et al. 2017, *MNRAS*, 466, 2825, doi: [10.1093/mnras/stw3270](https://doi.org/10.1093/mnras/stw3270)
- Cañameras, R., Nesvadba, N. P. H., Guery, D., et al. 2015, *A&A*, 581, A105, doi: [10.1051/0004-6361/201425128](https://doi.org/10.1051/0004-6361/201425128)
- Capak, P. L., Riechers, D., Scoville, N. Z., et al. 2011, *Nature*, 470, 233, doi: [10.1038/nature09681](https://doi.org/10.1038/nature09681)
- Carilli, C. L., & Walter, F. 2013, *ARA&A*, 51, 105, doi: [10.1146/annurev-astro-082812-140953](https://doi.org/10.1146/annurev-astro-082812-140953)
- Carniani, S., Maiolino, R., Smit, R., & Amorín, R. 2018, *ApJL*, 854, L7, doi: [10.3847/2041-8213/aaab45](https://doi.org/10.3847/2041-8213/aaab45)
- Casey, C. M., Narayanan, D., & Cooray, A. 2014, *PhR*, 541, 45, doi: [10.1016/j.physrep.2014.02.009](https://doi.org/10.1016/j.physrep.2014.02.009)
- Cormier, D., Madden, S. C., Lebouteiller, V., et al. 2015, *A&A*, 578, A53, doi: [10.1051/0004-6361/201425207](https://doi.org/10.1051/0004-6361/201425207)
- De Breuck, C., Weiß, A., Béthermin, M., et al. 2019, *A&A*, 631, A167, doi: [10.1051/0004-6361/201936169](https://doi.org/10.1051/0004-6361/201936169)
- Díaz, A. I., & Pérez-Montero, E. 2000, *MNRAS*, 312, 130, doi: [10.1046/j.1365-8711.2000.03117.x](https://doi.org/10.1046/j.1365-8711.2000.03117.x)
- Díaz-Santos, T., Armus, L., Charmandaris, V., et al. 2017, *ApJ*, 846, 32, doi: [10.3847/1538-4357/aa81d7](https://doi.org/10.3847/1538-4357/aa81d7)
- Fudamoto, Y., Smit, R., Bowler, R. A. A., et al. 2022, *ApJ*, 934, 144, doi: [10.3847/1538-4357/ac7a47](https://doi.org/10.3847/1538-4357/ac7a47)
- Fujimoto, S., Ouchi, M., Ferrara, A., et al. 2019, *ApJ*, 887, 107, doi: [10.3847/1538-4357/ab480f](https://doi.org/10.3847/1538-4357/ab480f)
- Genzel, R., Tacconi, L. J., Gracia-Carpio, J., et al. 2010, *MNRAS*, 407, 2091, doi: [10.1111/j.1365-2966.2010.16969.x](https://doi.org/10.1111/j.1365-2966.2010.16969.x)
- Ginolfi, M., Jones, G. C., Béthermin, M., et al. 2020, *A&A*, 633, A90, doi: [10.1051/0004-6361/201936872](https://doi.org/10.1051/0004-6361/201936872)
- Herrera-Camus, R., Bolatto, A. D., Wolfire, M. G., et al. 2015, *ApJ*, 800, 1, doi: [10.1088/0004-637X/800/1/1](https://doi.org/10.1088/0004-637X/800/1/1)
- Howell, J. H., Armus, L., Mazzarella, J. M., et al. 2010, *ApJ*, 715, 572, doi: [10.1088/0004-637X/715/1/572](https://doi.org/10.1088/0004-637X/715/1/572)
- Iverson, R. J., Smail, I., Le Borgne, J. F., et al. 1998, *MNRAS*, 298, 583, doi: [10.1046/j.1365-8711.1998.01677.x](https://doi.org/10.1046/j.1365-8711.1998.01677.x)
- Kashino, D., Silverman, J. D., Sanders, D., et al. 2017, *ApJ*, 835, 88, doi: [10.3847/1538-4357/835/1/88](https://doi.org/10.3847/1538-4357/835/1/88)
- Kennicutt, Robert C., J. 1998, *ARA&A*, 36, 189, doi: [10.1146/annurev.astro.36.1.189](https://doi.org/10.1146/annurev.astro.36.1.189)
- Kewley, L. J., Nicholls, D. C., & Sutherland, R. S. 2019, *ARA&A*, 57, 511, doi: [10.1146/annurev-astro-081817-051832](https://doi.org/10.1146/annurev-astro-081817-051832)
- Le Fèvre, O., Béthermin, M., Faisst, A., et al. 2020, *A&A*, 643, A1, doi: [10.1051/0004-6361/201936965](https://doi.org/10.1051/0004-6361/201936965)
- Marrone, D. P., Spilker, J. S., Hayward, C. C., et al. 2018, *Nature*, 553, 51, doi: [10.1038/nature24629](https://doi.org/10.1038/nature24629)
- Miller, T. B., Chapman, S. C., Aravena, M., et al. 2018, *Nature*, 556, 469, doi: [10.1038/s41586-018-0025-2](https://doi.org/10.1038/s41586-018-0025-2)
- Murphy, E. J., Condon, J. J., Schinnerer, E., et al. 2011, *ApJ*, 737, 67, doi: [10.1088/0004-637X/737/2/67](https://doi.org/10.1088/0004-637X/737/2/67)
- Pérez-Montero, E., & Contini, T. 2009, *MNRAS*, 398, 949, doi: [10.1111/j.1365-2966.2009.15145.x](https://doi.org/10.1111/j.1365-2966.2009.15145.x)
- Pettini, M., & Pagel, B. E. J. 2004, *MNRAS*, 348, L59, doi: [10.1111/j.1365-2966.2004.07591.x](https://doi.org/10.1111/j.1365-2966.2004.07591.x)
- Polletta, M., Weedman, D., Hönig, S., et al. 2008, *ApJ*, 675, 960, doi: [10.1086/524343](https://doi.org/10.1086/524343)
- Rizzo, F., Vegetti, S., Powell, D., et al. 2020, *Nature*, 584, 201, doi: [10.1038/s41586-020-2572-6](https://doi.org/10.1038/s41586-020-2572-6)
- Saintonge, A., Lutz, D., Genzel, R., et al. 2013, *ApJ*, 778, 2, doi: [10.1088/0004-637X/778/1/2](https://doi.org/10.1088/0004-637X/778/1/2)
- Sanders, D. B., & Mirabel, I. F. 1996, *ARA&A*, 34, 749, doi: [10.1146/annurev.astro.34.1.749](https://doi.org/10.1146/annurev.astro.34.1.749)
- Sanders, R. L., Jones, T., Shapley, A. E., et al. 2020, *ApJL*, 888, L11, doi: [10.3847/2041-8213/ab5d40](https://doi.org/10.3847/2041-8213/ab5d40)
- Scott, K. S., Austermann, J. E., Perera, T. A., et al. 2008, *MNRAS*, 385, 2225, doi: [10.1111/j.1365-2966.2008.12989.x](https://doi.org/10.1111/j.1365-2966.2008.12989.x)
- Spilker, J. S., Marrone, D. P., Aravena, M., et al. 2016, *ApJ*, 826, 112, doi: [10.3847/0004-637X/826/2/112](https://doi.org/10.3847/0004-637X/826/2/112)
- Steidel, C. C., Rudie, G. C., Strom, A. L., et al. 2014, *ApJ*, 795, 165, doi: [10.1088/0004-637X/795/2/165](https://doi.org/10.1088/0004-637X/795/2/165)
- Strom, A. L., Rudie, G. C., Steidel, C. C., & Trainor, R. F. 2022, *ApJ*, 925, 116, doi: [10.3847/1538-4357/ac38a3](https://doi.org/10.3847/1538-4357/ac38a3)
- Strom, A. L., Steidel, C. C., Rudie, G. C., Trainor, R. F., & Pettini, M. 2018, *ApJ*, 868, 117, doi: [10.3847/1538-4357/aae1a5](https://doi.org/10.3847/1538-4357/aae1a5)
- Tacconi, L. J., Genzel, R., & Sternberg, A. 2020, *ARA&A*, 58, 157, doi: [10.1146/annurev-astro-082812-141034](https://doi.org/10.1146/annurev-astro-082812-141034)
- THE CASA TEAM, Bean, B., Bhatnagar, S., et al. 2022, *arXiv e-prints*, arXiv:2210.02276, <https://arxiv.org/abs/2210.02276>
- Vieira, J. D., Marrone, D. P., Chapman, S. C., et al. 2013, *Nature*, 495, 344, doi: [10.1038/nature12001](https://doi.org/10.1038/nature12001)
- Viironen, K., Delgado-Inglada, G., Mampaso, A., Magrini, L., & Corradi, R. L. M. 2007, *MNRAS*, 381, 1719, doi: [10.1111/j.1365-2966.2007.12357.x](https://doi.org/10.1111/j.1365-2966.2007.12357.x)
- Vincenzo, F., Belfiore, F., Maiolino, R., Matteucci, F., & Ventura, P. 2016, *MNRAS*, 458, 3466, doi: [10.1093/mnras/stw532](https://doi.org/10.1093/mnras/stw532)

- Vishwas, A. 2019, PhD thesis, Cornell University, New York
- Weiß, A., De Breuck, C., Marrone, D. P., et al. 2013, ApJ, 767, 88, doi: [10.1088/0004-637X/767/1/88](https://doi.org/10.1088/0004-637X/767/1/88)